Korean J. Chem. Eng., **29**(3), 304-309 (2012)
DOI: 10.1007/s11814-011-0189-z

Intrinsic kinetics of the Fischer-Tropsch synthesis over an impregnated cobalt-potassium catalyst

Hossein Atashi*,†, Mohsen Mansouri*,, Seyyed Hossein Hosseini**, Mohammad Khorram*, Ali Akbar Mirzaei***, Masoud Karimi*, and Ghobad Mansouri******

*Department of Chemical Engineering, University of Sistan & Baluchestan, Zahedan 98164-161, Iran
**Department of Chemical Engineering, University of Ilam, Ilam 69315-516, Iran
***Department of Chemistry, University of Sistan & Baluchestan, Zahedan 98164-161, Iran
****Department of Chemistry, Islamic Azad University (Branch of Kermanshah), Kermanshah 6718997551, Iran
(*Received 15 May 2011 • accepted 28 July 2011*)

Abstract−The optimal amount of 15 wt%Co/10 wt%K/Al_2O_3 catalyst was prepared using the impregnation technique in order to study the kinetics of the Fischer-Tropsch synthesis. The rate of synthesis was measured in a fixed-bed micro reactor with H_2/CO feed ratio of 1-3 and space velocity in the range of 2,700-5,200 h^{-1} under reactor pressure of 8 bar and a temperature range of 210-240 °C. The experimental data were best fitted by a Langmuir-Hinshelwood-Hougen-Watson (LHHW) approach rate in the form of $-r_{CO}=(k_2K_1P_{CO}P_{H_2})/(1+K_1P_{CO})$. Furthermore, the data were fitted fairly well by a power law equation in the form of $-r_{CO}=kP_{CO}^{1.32}P_{H_2}^{1.42}$. The activation energies for LHHW approach model and power law equation were obtained as 138.5 kJ/mol and 87.39 kJ/mol, respectively.

Key words: Fischer-Tropsch Synthesis, Co/K/Al_2O_3 Catalyst, Fixed-bed Reactor, Kinetic Modeling, Impregnation Technique

INTRODUCTION

The Fischer-Tropsch synthesis (FTS) converts synthesis gas in a product spectrum consisting of a complex multicomponent mixture of linear and branched hydrocarbons and oxygenated products [1,2]. The FTS has the potential for producing chemical feedstocks or motor fuels without the production of the environmentally harmful compounds encountered in direct hydrogenation [3]. In general, modern FT synthesis is conducted through the gas phase-fixed bed system, the gas phase-fluidized bed system or the liquid phase-slurry system [4]. It is well known that VIII group metals can be used as a catalyst for FT reactions [5]. It has been found that the several metals such as nickel, cobalt, ruthenium and iron can be activated for FT reaction [6]. However, only iron and cobalt-based catalysts appear to be feasible and suitable on an industrial scale economically [6]. The cobalt catalysts are preferred for FTS due to their activity, high selectivity to long chain hydrocarbons and low activity for the side reactions such as competitive water-gas shift reaction [7]. Supported Co catalysts with high specific rates require the synthesis of small metal crystallites at high local surface densities on support and the use of supports or alloys that increase the rate per surface Co (turnover rate). Cobalt and Iron-based catalysts often contain small amounts of potassium and other metals such as manganese, calcium, zinc, copper and magnesium as promoters to improve their activity and selectivity [8]. Due to its stronger basicity, potassium has a stronger influences on adsorption of reactants (CO and H_2) on the active sites, and leads to improvements in FTS activity, enhancement in selectivity to olefins, suppression of methane formation and a selectivity shift to higher molecular weight products [9,10].

†To whom correspondence should be addressed.
E-mail: h.ateshi@hamoon.usb.ac.ir

The kinetic description of the FT reaction is very important for industrial practice, being a prerequisite for industrial process design, optimization and simulation. The kinetics of cobalt-based FT catalysts has been a subject of researches for decades. The mechanistic kinetic rate expressions for cobalt catalysts are based on the formation of the monomer species as the rate-determining step in the consumption of synthesis gas. Many kinetic equations have been proposed in the literature for various cobalt catalysts, and these have been obtained either empirically (using a power-law rate equation) or to fit a proposed mechanism [11-19]. A list of published kinetic models for the rate of FTS over various cobalt catalysts is given in Table 1.

In the present study, Fischer-Tropsch synthesis has been investigated over an active cobalt-potassium catalyst, which was prepared by impregnation method. For kinetic study, a series of statistically representative kinetic data was obtained on a well-characterized gamma-alumina supported catalyst over a range of commercially reaction conditions. The intrinsic kinetics of FT reaction was studied and the rate expressions were tested against the experimental data that was obtained on the selected catalysts. An appropriate model was successfully devised and the kinetics parameters were determined. Also, a power law kinetic equation for the carbon monoxide rate was obtained.

EXPERIMENTAL

1. Catalyst Preparation

The optimal amount of 15 wt%Co/10 wt%K/Al_2O_3, which has a high value of olefin/paraffin ratio and the chain growth probability, was prepared by impregnation method with an aqueous solution of $Co(NO_3)_2{\cdot}6H_2O$ and KNO_3 to incipient wetness of γ-Al_2O_3. The γ-alumina had been previously calcined at 400 °C for 8 h to

Table 1. Summary of kinetic studies of the FTS on cobalt catalysts

Reference	Catalyst	Reactor type[a]	T, k	P, bar	H_2/CO	Intrinsic kinetic expression[b] $(-r_{CO})$
[11]	Co	FBR	473-483	1-30	1-10	$\frac{kP_{CO}^{0.65}P_{H_2}^{0.6}}{(1+aP_{CO})}$
[12]	Co/kieselguhr	Berty	463	2-15	0.5-8.3	$\frac{kP_{CO}P_{H_2}^{0.5}}{(1+aP_{CO}+bP_{H_2}^{0.5})^2}$
[13]	$Co/MgO/SiO_2$	Slurry	493-513	5-15	1.5-3.5	$\frac{kP_{CO}P_{H_2}}{(1+aP_{CO})^2}$
[14]	$Co/CuO/Al_2O_3$	FBR	508-543	1.7-55	1-3	$kP_{CO}^{-0.5}P_{H_2}$
[15]	Co/ThO_2/kieselguhr	FBR	459-480	1	0.9-3.5	$\frac{kP_{CO}P_{H_2}^2}{(1+aP_{CO}P_{H_2}^2)}$
[16]	$Co/MgO/ThO_2$/kieselguhr	FBR	445-473	1	2	$kP_{CO}^{-1}P_{H_2}^2$
[17]	$Co/Pt/Al_2O_3$	Slurry	503	5-40	1.6-3.2	$\frac{kP_{CO}^{0.5}P_{H_2}^{0.75}}{(1+aP_{CO}^{0.5}P_{H_2}^{0.25}+bP_{CO}^{0.5}P_{H_2}^{-0.25})^2}$
[18]	$Co/Ru/Al_2O_3$	FBR	508-523	45-65	1.7-2.3	$\frac{kP_{CO}^{0.5}P_{H_2}^{0.5}}{(1+aP_{H_2}^{0.5}+bP_{CO}^{0.5}+cP_{CO})^2}$
[19]	Co/TiO_2	FBR	473	8-16	1-4	$\frac{kP_{CO}P_{H_2}^{0.74}}{(1+aP_{CO})^2}$

[a]FBR= Fixed-bed reactor

[b]k, b and c are temperature-dependent constants

remove the surface adsorbed impurities (BET surface area of 217 m^2/g, pore volume of 0.7 cm^3/g). The impregnated sample was dried at 110 °C for 2 h and calcined in air at 400 °C for 8 h (heating rate of 10 °C between 110 and 400 °C).

2. Fixed Bed Micro Reactor System

Fischer-Tropsch synthesis was carried out in a fixed-bed microreactor made of stainless steel with an inner diameter of 12 mm. Three mass flow controllers (Brooks, Model, 5850E) were used to adjust automatically flow rate of the inlet gases comprising CO, H_2 and N_2 (purity of 99.999%). A mixture of CO, H_2 and N_2 was subsequently introduced into the reactor, which was placed inside a tubular furnace (Atbin, Model ATU 150-15). The temperature of the reaction was controlled by a thermocouple inserted into the catalytic bed and visually monitored by a computer. The catalyst was in situ pre-reduced at atmospheric pressure under H_2-N_2 flow (N_2/H_2=1, flow rate of each gas=30 ml/min), at 400 °C for 16 h. In each test, 1.0 g catalyst was loaded and the reactor operated about 12 h to ensure attaining the steady state operating conditions.

3. Catalytic Evaluation

To derive the kinetic equations of intrinsic rate, which are ad-

Table 2. Summary of experimental conditions and results at P_{Tot}=8 bar and T=210-240 °C after 10-15 h of reaction at each given condition in a fixed bed reactor (FBR)

Number of data	Temperature (K)	X_{CO} (%)	P_{H_2} (bar)	P_{CO} (bar)	F/W (mol/gr cat. h)	$-r_{CO}$ (mmol/gr cat. h)
1	483.15	2.6	2.81	1.95	0.172	4.471
2	483.15	3.2	2.35	2.90	0.173	5.55
3	483.15	3.6	3.55	1.93	0.154	5.528
4	483.15	4.8	2.25	3.81	0.139	6.659
5	493.15	3.2	3.05	1.94	0.289	9.254
6	493.15	2.4	1.41	1.95	0.195	4.687
7	493.15	5.3	3.33	2.84	0.287	15.20
8	493.15	2.8	2.59	0.97	0.143	4.002
9	503.15	5.1	1.81	1.90	0.186	9.505
10	503.15	7.9	4.73	1.84	0.355	28.01
11	503.15	5.5	3.61	1.42	0.272	14.94
12	503.15	6.7	2.23	2.80	0.286	19.16
13	513.15	8.8	2.88	3.65	0.698	61.42
14	513.15	7.6	3.63	2.31	0.650	49.42
15	513.15	7.1	3.41	1.86	0.520	36.92
16	513.15	8.6	4.58	2.29	0.712	61.22

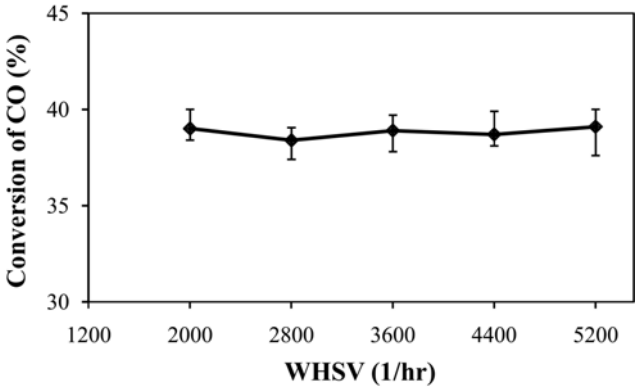

Fig. 1. Variation of the CO conversion, as a function of the WHSV value. Conditions: T=513 K, P=8 bar.

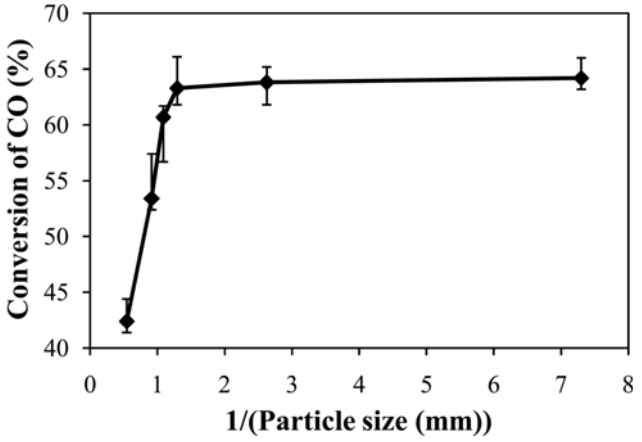

Fig. 2. Variation of the CO conversion as a function particle size. Conditions: T=513 K, P=8 bar, WHSV=3,600 h^{-1}.

justed with the experimental data, provided in Table 2, it should be noted that internal and external porous mass transfer resistances are not the controller and only the rate of surface reaction in the reactors is the controller. To check the external transport resistances, the feed flow rate was changed with a corresponding change in catalyst loading, so that a constant space velocity was achieved. Because the points corresponding to the same weight hourly space velocity (WHSV) have different flow rates closed together, thus, film resistance is not considerable. As can be seen in Fig. 1, over the range of interest film resistance is not signicant.

To examine the internal diffusion resistance, 1.0 g of catalyst with different sizes of 0.137, 0.381, 0.774, 0.92, 1.095 and 1.84 mm, which were smaller than those reported for the development of FTS reaction kinetics by the other researchers [20-23], was loaded under the same conditions. As shown in Fig. 2 no pore diffusion was evident for the particle size lower than 0.774 mm. In this study, the size of utilized catalyst is in the range of 0.26-0.38 mm.

Experiments were conducted with mixtures of H_2, CO and nitrogen in a temperature range of 210 to 240 °C at the H_2/CO feed ratios of 1/1-3/1 (mol/mol). The experimental data (CO conversions and CO consumption rates) obtained for 16 different activity tests of the 15 wt%Co/10 wt%K/Al_2O_3 catalyst in the FB reactor under reactor pressure of 8 bar and space velocity in the range of 2,700-5,200 h^{-1} after 10-15 h of reaction to obtain a steady-state activity, are summarized in Table 2.

To avoid the effects of deactivation, fresh catalysts were loaded for all experiments. To achieve isothermal conditions in the catalytic bed, the catalysts were diluted with an inert material (quartz). Axial temperature distribution was ensured using Mear's criterion [24,25] with $L/d_p>50$. In addition, plug-flow was assumed for the gaseous feed. The experimental reaction rate was determined by:

$$\text{Rate of CO conversion} = \frac{(\text{fractional conversion})\times(\text{input flow rate of CO})}{\text{weight of the catalyst}} \quad (1)$$

4. Optimization Method

To estimate the parameters of the kinetic model, the Levenberg-Marquardt (LM) algorithm still plays an important role. A non-linear regression algorithm of LM was utilized to fit the rival rate expressions to the experimental results by minimizing the summation of the squares of the differences as follows and estimation of the reaction rate constants:

$$f_{i,obj}=\sum_{i=1}^{N}\left(\frac{r_i^{exp}-r_i^{cal}}{r_i^{exp}}\right)^2 \quad (2)$$

The discrimination between the rival models is based on the mean absolute relative residuals (MARR), which are calculated by:

$$MARR=\frac{1}{N_{exp}}\sum_{i=1}^{N_{exp}}\left(\frac{\left|r_i^{exp}-r_i^{cal}\right|}{r_i^{exp}}\right)\times 100 \quad (3)$$

The rate of models yielding negative adsorption coefficients was excluded and estimated kinetic parameters should have a physical relevance. The R^2 value (reflects the amount of variance) and root mean of standard deviation (Rmsd) of the involved rate measurement are reported as measure of the goodness of fit:

$$\sigma=\frac{1}{N_{exp}}\sum_{i=1}^{N_{exp}} r_{CO,i}^{exp} \quad (4)$$

$$R^2=1-\left(\frac{\sum_{i=1}^{N_{exp}}\left(r_{CO,i}^{exp}-r_{CO,i}^{cal}\right)^2}{\sum_{i=1}^{N_{exp}}\left(r_{CO,i}^{exp}-\sigma\right)^2}\right)^2 \quad (5)$$

$r_{CO,i}^{exp}$ and $r_{CO,i}^{cal}$ indicate the experimental and calculated CO conversion rate from each kinetic model in *i*th data point, respectively, and N_{exp} clarify the number of experimental data points with pure error variance σ.

RESULTS AND DISCUSSION

1. Development of Kinetic Equations

The mechanism of the hydrocarbon formation during the FTS has been reviewed and discussed by several authors [11-19]. The most important growth mechanism for the hydrocarbon formation is the surface carbide mechanism by CH_2 insertion. To derive the rate equations that should be adjusted with the data provided in Table 2, the LHHW model was used to obtain the kinetic models. According to this theory, a reaction mechanism should be adopted. Four mechanisms were offered on the basis of various monomer formation (elementary reactions) and carbon chain distribution pathways.

Table 3. Elementary reactions mechanism set for FTS

Model	Number	Elementary reaction
FT-I	1	$CO+s \leftrightarrow COs$
	2	$COs+s \leftrightarrow Cs+Os$
	3	$H_2+2s \leftrightarrow 2Hs$
	4	$Cs+Hs \leftrightarrow CHs+s$
	5	$CHs+Hs \leftrightarrow CH_2s+s$
	6	$Os+Hs \rightarrow HOs+s$
	7	$HOs+Hs \rightarrow H_2Os+s$
	8	$H_2O+s \rightarrow H_2Os$
FT-II	1	$CO+s \leftrightarrow COs$
	2	$COs+s \leftrightarrow Cs+Os$
	3	$Cs+H_2 \rightarrow CH_2s$
	4	$Os+H_2 \rightarrow H_2Os$
	5	$H_2O+s \rightarrow H_2Os$
FT-III	1	$CO+s \leftrightarrow Cos$
	2	$H_2+2s \leftrightarrow 2Hs$
	3	$COs+Hs \leftrightarrow HCOs+s$
	4	$HCOs+Hs \leftrightarrow Cs+H_2Os$
	5	$Cs+Hs \leftrightarrow CHs+s$
	6	$CHs+Hs \leftrightarrow CH_2s+s$
	7	$H_2O+s \rightarrow H_2Os$
FT-IV	1	$CO+s \leftrightarrow COs$
	2	$COs+H_2 \leftrightarrow H_2COs$
	3	$H\text{-}COs+H_2 \leftrightarrow CH_2s+H_2O$
	4	$H_2O+s \rightarrow H_2Os$

Table 4. Reaction rate expressions for the FTS, r_{FT} ($mmolg_{cat}^{-1}h^{-1}$)

Model of rate controlling	Kinetic equation
FT-I1	$kP_{CO}/(1+aP_{CO}^{1/2}+bP_{H_2}^{1/2})$
FT-I3	$kP_{H_2}/(1+aP_{CO}^{1/2}+bP_{H_2}^{1/2})^2$
FT-I4	$kP_{CO}^{1/2}P_{H_2}^{1/2}/(1+aP_{CO}^{1/2}+bP_{H_2}^{1/2})^2$
FT-I5	$kP_{CO}^{1/2}P_{H_2}^{3/4}/(1+aP_{CO}^{1/2}P_{H_2}^{-1/4}+bP_{H_2}^{1/2})^2$
FT-II1	$kP_{CO}/(1+aP_{CO}^{1/2})$
FT-II3	$kP_{CO}^{1/2}P_{H_2}/(1+aP_{CO}^{1/2})$
FT-III1	$kP_{CO}/(1+aP_{CO}+bP_{H_2}^{1/2})^{1/2}$
FT-III2	$kP_{H_2}/(1+aP_{CO}+bP_{H_2}^{1/2})^{1/2}$
FT-III3	$kP_{CO}P_{H_2}^{1/2}/(1+aP_{CO}+bP_{H_2}^{1/2})^{1/2}$
FT-III4	$kP_{CO}P_{H_2}/(1+aP_{CO}+bP_{H_2}^{1/2})^{1/2}$
FT-IV1	$kP_{CO}/(1+aP_{CO})$
FT-IV2	$kP_{CO}P_{H_2}/(1+aP_{CO})$
FT-IV3	$kP_{CO}P_{H_2}^2/(1+aP_{CO})$

The elementary reactions, which have been settled on sites for different models are listed in Table 3.

To derive each kinetic model, first one elementary reaction (in some cases two or three) was assumed as the rate-determining step and all other steps were considered at equilibrium state. Then, all of the models obtained were fitted separately against the experimental data. In the interest of conciseness, only certain selected kinetic models are reported in Table 4.

For example, derivation of the rate equation for FT-IV2 is explained here. For doing this work, the FT-IV2 step is considered as the determinant rate of reaction and its reaction is assumed as irreversible. The other steps can be considered as quick and at equilibrium.

The rate expression for the FT-IV2 model, where adsorbed CO reacts with molecular hydrogen as determinant rate of reaction, can be stated as irreversible adsorption by:

$$-r_{CO}=k_2\theta_{CO}P_{H_2} \tag{6}$$

where $-r_{CO}$ is the rate of disappearance of CO, k_2 is the forward rate constant for adsorbed CO that reacts with the molecular hydrogen, P_{H_2} is hydrogen partial pressure in the gas phase, and θ_{CO} is the surface fraction occupied with the associative absorbed carbon monoxide. The fraction of vacant sites, θ_S, can be calculated from the following balance equation:

$$\theta_S+\theta_{CO}+\theta_{H_2CO}+\theta_{CH_2}+\theta_{H_2O}=1 \tag{7}$$

Hydrogen and carbon monoxide are adsorbed dissociatively on the cobalt catalyst depending on the catalyst and reaction conditions, while the extent of dissociation of CO is varied [26]. However, CO is adsorbed more strongly than hydrogen [27]. In this case, it is assumed that only CO occupies the major of total number of sites. Other species were assumed to be negligible in the stoichiometric balance:

$$\theta_S+\theta_{CO}=1 \tag{8}$$

The surface coverage of carbon monoxide is calculated from the site balance, and the preceding reaction steps, which are at quasi-equilibrium:

$$CO+S \xrightarrow{k_1} COs \tag{9}$$

$$k_1P_{CO}\theta_S-k_{1,des}\theta_{CO}=0 \tag{10}$$

$$\theta_{CO}=K_1P_{CO}\theta_S \tag{11}$$

$$K_1=\frac{k_1}{k_{1,des}}$$

where K_1 is the equilibrium constant of CO adsorption step. By substituting Eq. (11) into Eq. (8), the ratio of free active site can be expressed as follows:

$$\theta_S=\frac{1}{1+K_1P_{CO}} \tag{12}$$

Finally, by substitution of the vacant sites fraction in Eq. (6), the final rate expression is obtained as follows:

$$-r_{CO}=\frac{k_2K_1P_{CO}P_{H_2}}{1+K_1P_{CO}}=\frac{kP_{CO}P_{H_2}}{1+aP_{CO}} \tag{13}$$

Table 4 summarizes the final form of the different rate expressions for the 13 possible kinetic models, whereas Table 5 shows the kinetic and adsorption parameters for the several kinetic models. It can be seen that the pressure dependency of CO and H_2 is in the range of 1/2 to 1, and 1/2 to 2, respectively. The denominator is quadratic in case of a dual-site elementary reaction, in contrast to a single-site rate-determining step. The denominator consists of the individual contributions of signicantly plentiful species on the catalyst surface.

In addition, the power law kinetic equation for the carbon monoxide rate was considered for comparison with the experimental

Table 5. Parameters and mean absolute relative residuals (MARR) for the FT kinetic models

Model of rate controlling	k (x) (mmol g^{-1} h^{-1} bar^x)	a (x) (bar^x)	b (x) (bar^x)	MARR (%)
FT-I1	k_1 (−1)	$(k_6K_1K_2/k_4)^{1/2}$ (−1/2)	$K_3^{1/4}$ (−1/2)	13.3
FT-I3	k_3 (−1)	$(k_6K_1K_2/k_4)^{1/2}$ (−1/2)	$K_3^{1/4}$ (−1/2)	12.7
FT-I4	$(k_4k_6K_1K_2K_3)^{1/2}$ (−1)	$(k_4K_1K_2/k_6)^{1/2}$ (−1)	$K_3^{1/4}$ (−1/2)	11.9
FT-I5	$(k_3k_6K_1K_2K_4)^{1/2}$ $k_3^{1/4}$(−5/4)	$(k_6K_1K_2/k_5K_4)^{1/2}$ $k_3^{-1/4}$ (−1/4)	$K_3^{1/4}$ (−1/2)	27.4
FT-II1	k_1 (−1)	$(K_1K_2K_4/k_3)^{1/2}$ (−1/2)		24.0
FT-II3	$(k_3k_4K_1K_2)^{1/2}$ (−3/2)	$(K_1K_2K_4/k_3)^{1/2}$ (−1/2)		10.9
FT-III1	k_1 (−1)	K_1 (−1)	$k_2^{1/2}$ (−1/2)	16.3
FT-III2	k_2 (−1)	K_1 (−1)	$k_2^{1/2}$ (−1/2)	21.5
FT-III3	$(k_3K_1K_2^{1/4})^{1/2}$ (−3/2)	K_1 (−1)	$k_2^{1/2}$ (−1/2)	19.1
FT-III4	$(k_4K_1K_2K_3)$ (−2)	K_1 (−1)	$k_2^{1/2}$ (−1/2)	11.8
FT-IV1	k_1 (−1)	K_1 (−1)		18.8
FT-IV2	k_2K_1 (−2)	K_1 (−1)		9.2
FT-IV3	$k_2K_1K_2$ (−3)	K_1 (−1)		13.6

data.

Yang et al. [14] and Zennaro et al. [19] obtained empirical rate expressions for supported cobalt catalysts using a fixed-bed reactor via regression of a power-law equation in the general form of:

$$-r_{CO} = k_0 \exp\left(\frac{-E}{RT}\right) P_{CO}^m P_{H_2}^n \quad (14)$$

where P_{CO} stands for partial pressure of carbon monoxide, k_0 stands for the reaction rate constant, E for the activation energy of CO consumption, m for the reaction order of CO and n for the reaction order of H_2.

2. Model Parameters and Model Discrimination

CO consumption rate was obtained from the data provided in Table 2 by using the differential method of data analysis. The kinetic data presented in Table 2 for CO conversion were used for testing the power law equation and thirteen models listed in Table 4. The least square method and non-linear regression analysis based on the summarized values in Table 2 are used to determine the power-law equation parameters and kinetic model parameters from the experimental data provided in Table 3. Arrhenius and adsorption equations were substituted in kinetics models: Eqs. (15) and (16) were substituted for k and a, respectively.

$$k = k_0 \exp\left(\frac{-E}{RT}\right) \quad (15)$$

$$a = a_0 \exp\left(\frac{\Delta H}{RT}\right) \quad (16)$$

Considering the different surface reaction mechanisms and rate determination steps, 13 kinetic models (see Table 4) were obtained and evaluated. The rival rate expressions of Table 2 were fitted to the experimental data by minimizing the relative variance. The parameter of the kinetic models and a number of statistical indicators are listed in Table 5.

Table 5 shows the parameters and mean absolute relative residuals (MARR) for the FT kinetic models. It can be seen that the FT-IV2 model has the lowest relative variance among the other models that have been used in the present study. Thereupon, the FT-IV2 model that has the minimal MARR value fits the experimental data well and has less deviation from the experimental data. Therefore, they are best fitted by an LHHW approach rate form $-r_{CO}=(kP_{CO}P_{H_2})/(1+aP_{CO})$ with combined enol/carbide mechanism as the rate-controlling step, where the obtained activation energy is equal to 138.5 kJ/mol.

Fig. 3 shows a comparison between the experimental data and

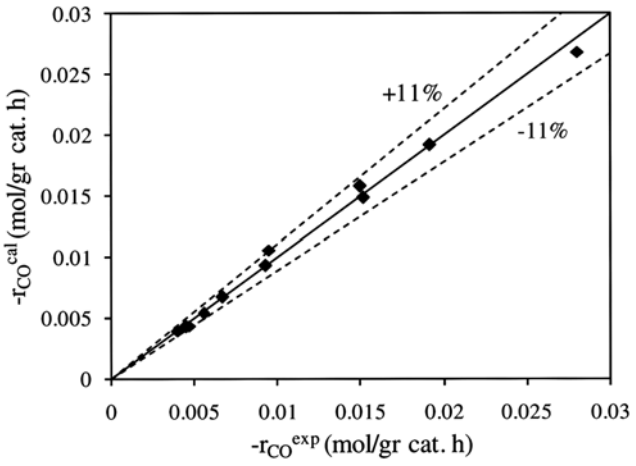

Fig. 3. A comparison between the experimental data with predicted results of the FT-IV2 model equation.

Table 6. Values of the kinetic parameters, activation energy and heat of adsorption of CO with various equations

Equation	k_0 (mol·gCat^{-1}·h^{-1}·bar^x)	E (kJ/mol)	a_o ($bar^{-0.5}$)	ΔH (kJ/mol)	m (-)	n (-)
[a]FT-IV2	7.49×10^{11}	138.5	1.00	−25.56		
[b]Power law	1.87×10^{6}	87.39			1.32	1.42

x: a=−2, b=−2.74

predicted results of the FT-IV2 model. The solid line in the figure denotes that calculated $-r_{CO}$ is equal to the experimental one and dotted lines over and under the solid line represent 11% deviation. The experimental results were found in good agreement with the optimal kinetic model showing about 11% deviation.

The data of this study are fitted fairly well by a power law equation in the form of $-r_{CO}=1.87\times10^{6}\exp((-8.74\times10^{4})/RT)P_{CO}^{1.32}P_{H_2}^{1.42}$. The R^2 value has been obtained as 0.99, which shows the power law equation is well matched with the experimental data. Table 6 shows the kinetic parameters calculated for the kinetic FT-IV2 model and power law equation. The activation energy is different for the two proposed models. It may be due to the other constant coefficients, which affect the activation energy of power law equation significantly.

CONCLUSION

Cobalt-potassium catalyst was prepared by impregnation method and the experiments were carried out in a stainless steel microreactor. The kinetic model of FTS reaction over a well-characterized 15%wtCo/10%wtK/Al_2O_3 catalyst, which is used as an optimized catalyst of the process, was studied. The data of this study are best fitted by the simple LHHW approach rate of the form $-r_{CO}=(kP_{CO}P_{H_2})/(1+aP_{CO})$. The values of kinetic constants were obtained and the activation energy was found equal to 138.5 kJ/mol for the best model. The data are fitted fairly well by a power law equation in the form of $-r_{CO}=1.87\times10^{6}\exp((-8.74\times10^{4})/RT)P_{CO}^{1.32}P_{H_2}^{1.42}$.

SYMBOLS

L : length of catalytic bed [m]
d_p : particle diameter [m]
H_i : heat of adsorption of component I [kJ/mol]

REFERENCES

1. G. P. Van Der Laan and A. A. C. M. Beenackers, *Appl. Catal. A: Gen.*, **193**, 39 (2000).
2. H.-S. Song, D. Ramkrishna, S. Trinh and H. Wright, *Korean J. Chem. Eng.*, **21**, 308 (2004).
3. C. K. Rofer-Depoorter, *Chem. Rev.*, **81**, 447 (1981).
4. C.-U. Kim, Y.-S. Kim, H.-J. Chae, K.-E. Jeong, S.-Y. Jeong, K.-W. Jun and K.-Y. Lee, *Korean J. Chem. Eng.*, **27**, 777 (2010).
5. Y. H. Kim, D.-Y. Hwang, S. H. Song, S. B. Lee, E. D. Park and M.-J. Park, *Korean J. Chem. Eng.*, **26**, 1591 (2009).
6. A. N. Pour, Y. Zamani, A. Tavasoli, S. M. K. Shahri and S. A. Taheri, *Fuel*, **87**, 2004 (2008).
7. J.-K. Jeon, C.-J. Kim, Y.-K. Park and S.-K. Ihm, *Korean J. Chem. Eng.*, **21**, 365 (2004).
8. A. N. Pour, S. M. K. Shahri, H. R. Bozorgzadeh, Y. Zamani, A. Tavasoli and M. A. Marvast, *Appl. Catal. A: Gen.*, **348**, 201 (2008).
9. Y. Yang, H. W. Xiang, Y. Y. Xu, L. Bai and Y. W. Li, *Appl. Catal. A: Gen.*, **266**, 181 (2004).
10. A. P. Raje, R. J. O. Brien and B. H. Davis, *J. Catal.*, **180**, 36 (1998).
11. E. Iglesia, S. C. Reyes and S. L. Soled, in: *Computer-Aided Design of Catalysts*, E. R. Becker, et al. Eds., Dekker, New York (1993).
12. B. Sarup and B. W. Wojciechowski, *Can. J. Chem. Eng.*, **74**, 62 (1989).
13. I. C. Yates and C. N. Sattereld, *Energy and Fuels*, **5**, 168 (1991).
14. C. H. Yang, F. E. Massoth and A. G. Oblad, *Adv. Chem. Ser.*, **178**, 35 (1979).
15. R. B. Anderson, in: *Catalysis*, P. H. Emmett Ed., Reinhold, New York (1956).
16. W. Brötz, *Z. Elektrochem.*, **5**, 301 (1949).
17. F. Gideon Botes, B. Van Dyk and C. Mcgregor, *Ind. Eng. Chem. Res.*, **48**, 10439 (2009).
18. A. Irankhah, A. Haghtalab, E. V. Farahani and K. Sadaghianizadeh, *J. Nat. Gas Chem.*, **16**, 115 (2007).
19. R. Zennaro, M. Tagliabue and C. Bartholomew, *Catal. Today*, **58**, 309 (2000).
20. E. F. G. Herington, *Chem. Ind.*, **65**, 346 (1946).
21. E. S. Lox, G. B. Marin, E. De Graeve and P. Bussier, *Appl. Catal. A*, **40**, 197 (1988).
22. G P. Vander Laan and A. A. C. M. Beenackers, *Catal. Rev. Sci. Eng.*, **41**, 255 (1999).
23. Y. N. Wang, W. P. Ma, Y. J. Lu, J. Yang, Y. Y. Xu, H. W. Xiang, Y. L. Zha and B. J. Zhang, *Fuel*, **82**, 195 (2003).
24. D. E. Mears, in: *Chemical Reaction Engineering II*, H. M. Hulburt Ed., ACS Monograph, Washington (1974).
25. M. Mollavali, F. Yaripour, H. Atashi and S. Sahebdelfar, *Ind. Eng. Chem. Res.*, **47**, 3265 (2008).
26. V. Ponec and W. A. Van Barnevald, *Ind. Eng. Chem. Prod. Res. Dev.*, **18**, 268 (1979).
27. K. Christman, O. Scober, G. Ertl and M. Neumann, *J. Chem. Phys.*, **60**, 4719 (1974).